**Title:** Post-Synthetic Selective Ligand Cleavage by Solid-Gas Phase Ozonolysis Fuses Micropores into Mesopores in Metal-Organic Frameworks

Authors: Vincent Guillerm,† Heng Xu,† Jorge Albalad,† Inhar Imaz†* and Daniel Maspoch†§*

Affiliations: † Catalan Institute of Nanoscience and Nanotechnology (ICN2), CSIC and The Barcelona Institute of Science and Technology, Campus UAB, Bellaterra, 08193 Barcelona, Spain; § ICREA, Pg. Lluís Companys 23, 08010 Barcelona, Spain

Keywords: Metal-Organic Frameworks (MOFs), Solid-Gas Reaction, Ozonolysis, Post Synthetic Modification, Multivariate MOFs, Mesoporosity, Adsorption, Olefin Chemistry.

TOC image:
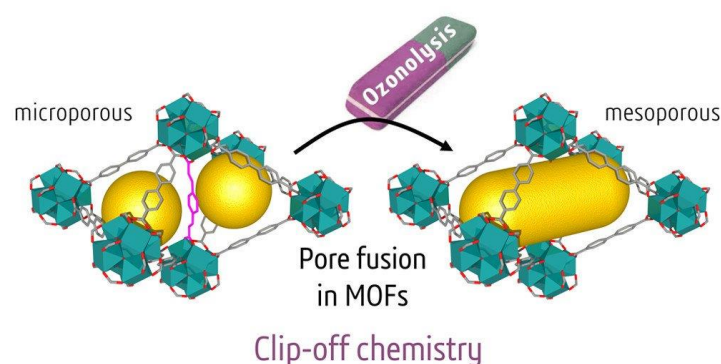
ABSTRACT

Herein we report a novel, ozone-based method for post-synthetic generation of mesoporosity in metal-organic frameworks (MOFs). By carefully selecting mixed-ligand Zr-fcu-MOFs based on organic ligand pairs in which one ligand has ozone-cleavable olefin bonds and the other ligand is ozone-resistant, we were able to selectively break the cleavable ligand via ozonolysis to trigger fusion of micropores into mesopores within the MOF framework. This solid-gas phase method is performed at room-temperature and, depending on the cleavable ligand used, the resultant ligand-fragments can be removed from the ozonated MOF by either washing or sublimation. Compared to the corresponding highly-microporous starting MOFs, the highly-mesoporous product MOFs exhibit radically distinct gas sorption properties.

INTRODUCTION

Since the advent of metal-organic frameworks (MOFs) in the late 1990's,[1] these porous materials have shown promise for critical applications[2] such as gas storage,[3] catalysis,[4] drug delivery,[5] thermal energy storage,[6] sensors,[7] etc. MOFs have become benchmark materials for adsorption, surpassing most traditional adsorbents for hydrogen storage,[3a] methane storage,[3b] CO_2/N_2 separation,[8] etc. By marrying the advantages of the inorganic and organic chemistries, MOFs exhibit both polyfunctionality and a high degree of tunability, as well as the opportunity to post-functionalize them.[9] Among the main advantage of this tunability is the possibility to perform reticular chemistry[1d, 10] through ligand functionalization, length/width[10g] variation, and/or metal ion substitution, which enables strategic design and synthesis of materials for specific applications.

A remaining challenge in MOF chemistry is the creation of mesoscale cavities, which are necessary for increased storage capacity, encapsulation of large molecules, etc. Reticular chemistry strategies to surpass previous limits on pore size and cavity diameter include increasing the distance between the organic molecular building blocks and using longer or wider organic ligands.[10e, 11] However, many of the most well-known MOFs are associated to self-dual nets (**pcu**: MOF-5,[1c] IRMOFs series,[1d] MXFSIX MOFs[12]) or nets that can easily interpenetrate upon ligand elongation (**tbo**: HKUST-1,[1e, 13] **fcu**: UiO-66,[14] **acs**: MIL-88's,[15] etc.). To avoid this problem, researchers have developed platforms based on topologies that cannot interpenetrate, such as IRMOFs-74[10e] and **rht**-MOFs[16], which, thanks to the design of very ambitious organic ligands, currently hold porosity records.[10e, 11b, 11d]

Regrettably, systematic access to MOFs exhibiting hierarchical porosity from the micro to the meso range remains a challenge, as it currently demands use of complex organic ligands that are not commercially available.[11c, 17] Although MOFs were initially considered as structurally ideal, defect-free materials, numerous recent studies have highlighted the non-negligible level of structural defects and irregularities in these materials, which strongly influence their porosity and catalytic properties.[17e, 18] These findings suggest that access to hierarchically porous materials would require rational control over the structural defects within MOFs. Unfortunately, to date, only a few methods for generating and controlling such defects have emerged. One such strategy is to use large amounts of monotopic agents (known as *modulators*) in competition with the required polytopic ligand corresponding to the targeted MOFs.[14b, 19] Alternatively, rational design strategies such as transversal reticular chemistry also have proven invaluable for generating MOFs with ordered defects.[10g] However, there are very few reports on engineering of defects and control of hierarchical porosity with commercially available and/or moderately sized ligands,[17e, 18e, 20] and some of the existing methods require harsh chemical or thermal treatments.

Our group recently reported the first solid-gas phase covalent post-synthetic modification of a MOF: under mild conditions, we achieved quantitative conversion of the constituent olefin groups in single crystals of UiO-66-like MOF into trioxolane moieties, aldehydes and/or carboxylates without compromising the crystallinity.[21] Encouraged by the stability of the MOFs under these conditions, we envisioned exploiting this solid-gas phase ozonolysis[22] method to cleave and remove selected organic ligands within MOFs. We hypothesized and later confirmed (*vide infra*) that ligands containing non-terminal olefin groups could be split into several parts (Scheme S1). When implemented in MOFs, these ligands can be selectively broken and subsequently removed from the framework, to provide an original and controllable method for post-synthetic fusion of micropores into mesopores.

Herein we report application of our post-synthetic strategy to selectively and quantitatively cleave and remove the organic ligands in two multivariate (MTV)[23] Zr-**fcu**-MOFs (Figure 1), thereby affecting their adsorption performance in gas uptake. By controlling the ozone inert/active ratio of ligands in these MOFs, we were able to control the final number of defects in their structures.
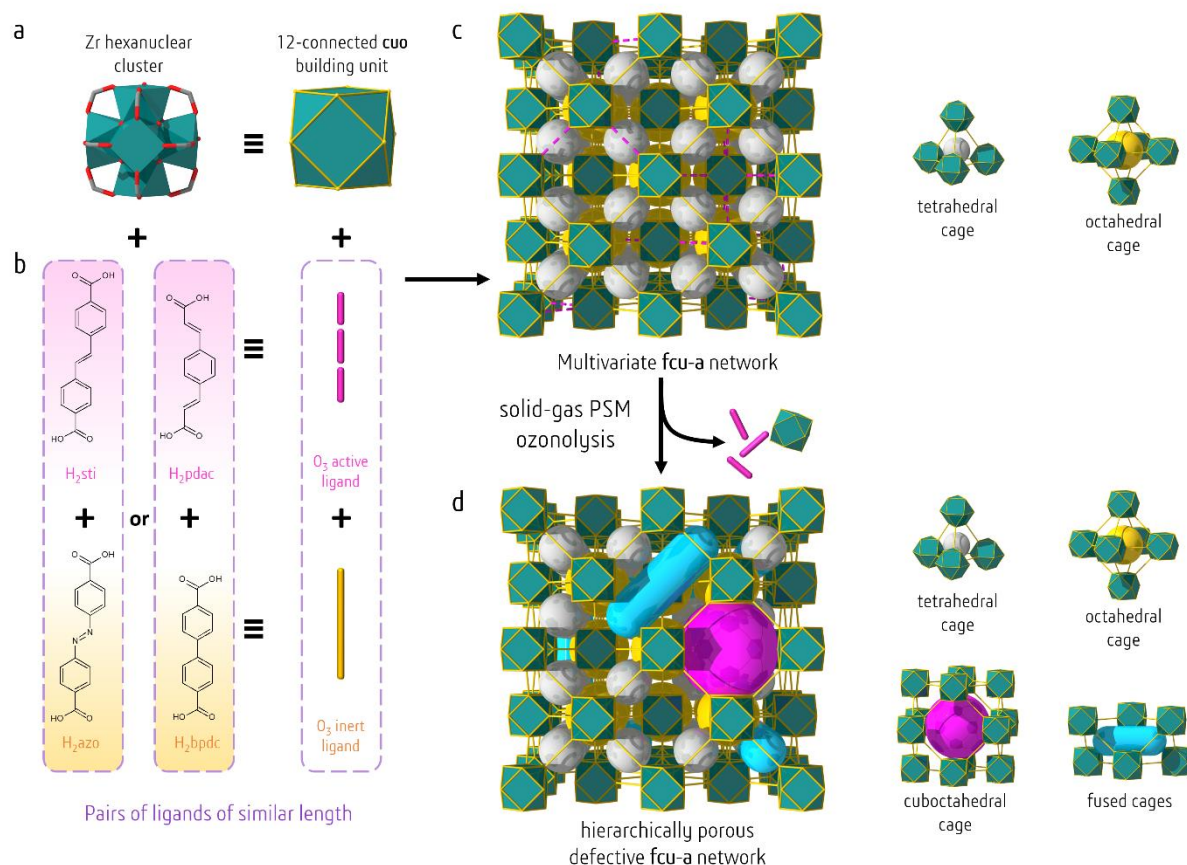
Figure 1. Post-synthetic modification of multivariate Zr-**fcu**-MOFs via solid-gas ozonolysis. Reaction of a) 12-connected hexanuclear clusters (**cuo** molecular building blocks) with b) pairs of organic ligands that are similar in length but show opposite reactivity to ozone (H$_2$sti & H$_2$azo or H$_2$pdac & H$_2$bpdc) yields c) multivariate MOFs with the **fcu** topology and two types of cages. Post-synthetic modification of the resultant MOFs through ligand cleavage by solid-gas ozonolysis results in d) Zr-**fcu**-MOFs with a defective network that exhibits hierarchical porosity generated upon fusion of micropores into larger pores (up to the meso scale).

RESULTS AND DISCUSSION

Zr-fcu-azo/sti system.

System validation. Our ligand-removal strategy is only amenable to MOFs based on ligand pairs that exhibit the following characteristics: similar shape and length; similar reactivity under given reaction conditions; and opposite reactivity to ozone (Figure 1b). To this end, we selected two dicarboxylic acids: 4,4'-azobenzene dicarboxylic acid (H$_2$azo) and 4,4'-stilbene dicarboxylic acid (H$_2$sti) (with lengths ≈ 13.3 Å). The reactivity of each ligand to ozone was initially tested in solution, in *N,N'*-dimethylformamide (DMF), which was used to avoid π-π stacking of the ligands and to facilitate access of the ozone molecules to the olefin groups. Interestingly, the two acids showed diametric responses to ozone: H$_2$azo was unreactive, whereas H$_2$sti was fully converted into terephthalic acid (H$_2$bdc) and formylbenzoic acid (Hfba) (Scheme S1, Figure S18).

Having confirmed the suitability of H$_2$azo and H$_2$sti as a ligand pair, we then decided to choose an appropriate MOF for testing. We selected the robust Zr-**fcu**-MOF platform, which had already proven amenable to post-synthetic modification and ozone resistant.[9b, 9d, 21, 24] Thus, we embarked on the synthesis of the resultant MOFs (Zr-**fcu**-azo[25] and Zr-**fcu**-sti[26]) and testing of their response to ozonolysis. Both MOFs were synthesized by suspending ZrCl$_4$ and the corresponding dicarboxylic ligand in DMF, in the presence of HCl and L-proline, and then heating the resulting mixture at 120 ºC

overnight in a scintillation vial. The resulting crystals (of Zr-**fcu**-azo or Zr-**fcu**-sti) were washed with DMF and then subjected to solvent exchange with acetone. As expected, N_2 sorption isotherms collected at 77 K confirmed comparable Brunauer-Emmett-Teller areas (A_{BET}) of 3025 m^2/g for Zr-**fcu**-azo and 3065 m^2/g for Zr-**fcu**-sti (Figure 2a). When submitted to ozone treatment for 30 min, Zr-**fcu**-azo retained its crystallinity and porosity, whereas Zr-**fcu**-sti collapsed into an amorphous, non-porous solid due to cleavage of all the ligands of the framework (Figures 2a, S2, S9).

Synthesis and porosity of Zr-fcu**-azo/sti-X%.** To prepare multivariate Zr-**fcu**-MOFs containing specific ratios of azo/sti (ranging from 90:10 to 40:60), we used similar synthetic conditions as for Zr-**fcu**-azo, but partially replaced the H_2azo with the appropriate amount of H_2sti. The phase purity of the resulting single crystals of Zr-**fcu**-azo/sti-X% (X ≈ 10, 20, 30, 40, 50 or 60 stilbene molar percentage) was confirmed by powder X-ray diffraction (PXRD; Figure 2b). The crystals varied in color from bright orange to colorless (Figure S1) according to their constituent azo/sti ratio, which was confirmed by proton nuclear magnetic resonance (^{1}H NMR) of digested crystals (Figure S19, Tables S1, S3). Finally, N_2 sorption analysis performed at 77 K showed comparable uptake and type I isotherm for all different activated samples (Figure 2e). Indeed, all apparent A_{BET} values ranged from 3000 m^2/g to 3065 m^2/g and total pore volumes, from 1.24 cm^3/g to 1.28 cm^3/g (Table 1). As expected, and similarly to reported values for comparable MOF systems,[18e] the pore size distributions (PSD, Figure 2h) of all Zr-**fcu**-azo/sti-X% are comparable: with a main pore population of ca. 18.4 Å attributed to the intrinsic porosity of the framework and a minor population of larger pores of ca. 22.4 Å attributed to some modulator related defects.

Table 1. Apparent BET area, micropore volume and total pore volume of Zr-**fcu**-azo/sti-X%, before and after ozonolysis & washing.

	Starting MOF			Ozonated & washed MOF		
initial% sti	A_{BET} (m^2/g)	V_μ (cm^3/g)	V_t (cm^3/g)	A_{BET} (m^2/g)	V_μ (cm^3/g)	V_t (cm^3/g)
0	3025	1.26	1.29	3030	1.24	1.27
10	3060	1.25	1.28	3115	1.27	1.32
20	3045	1.23	1.25	3130	1.31	1.38
30	3000	1.11	1.24	2680	1.17	1.38
40	3040	1.23	1.27	2580	1.10	1.44
50	3065	1.23	1.26	1860	0.79	1.36
60	3015	1.22	1.26	985	0.42	0.75
100	3065	1.26	1.31	Non-porous		

Ozonolysis of Zr-fcu**-azo/sti-X%.** To selectively break the sti ligands, we packed *ca.* 50 mg of Zr-**fcu**-azo/sti-X% into a L- shaped glass tube, connected on one side to the ozonator (through a $CaCl_2$ humidity trap), and on the other side, to a vacuum pump (through a KI trap), to ensure a continuous flow of ozone through the column. The reaction was run at room temperature for 30 min. The ozonated Zr-**fcu**-azo/sti-X% materials maintained their high crystallinity after ozonolysis, as confirmed by PXRD (Figures S2-S10). ^{1}H NMR of digested, Zr-**fcu**-azo/sti-X%_OZ confirmed the full conversion of sti into bdc and fba for all samples (Figure S20, Table S4). The 1:1 bdc/fba ratio observed for all Zr-**fcu**-azo/sti-X%_OZ also indicated the stoichiometric character of the reaction (Figures 2d, 3a). As expected, based on our preliminary results with Zr-**fcu**-azo, the content of azo ligand in the framework was not affected by ozonolysis, thus confirming its high selectivity towards olefin bonds.

Washing of Zr-fcu-**azo/sti-X%_OZ.** To remove the organic and inorganic fragments trapped in the pores of the Zr-**fcu**-azo/sti-X%_OZ, we washed the ozonated crude product in a 0.5 M solution of acetic acid in DMF. The washed samples did not exhibit any marked difference in crystallinity compared to the corresponding crude products, as confirmed by PXRD (Figure S10), with one exception: Zr-**fcu**-azo/sti-60%_OZ. The washing step revealed that the latter had indeed lost crystallinity, which we attributed to a partial collapse of its framework upon loss of 60% of its ligands via ozonolysis. In all cases, ^{1}H NMR (Figures S21, S22 and Tables S5, S6) of the washed Zr-**fcu**-azo/sti-X% revealed the absence of fba and the persistence of some bdc, which could not be fully removed (repeated washing did not remove any additional bdc).

Porosity properties of washed, ozonated Zr-fcu-**azo/sti-X%.** After confirming that in the washed, ozonated Zr-**fcu**-azo/sti-X%, all the sti ligands had been broken (Figure S20), most of the resulting organic fragments had washed out (Figure S21) and the high crystallinity had remained (Figure S10c), we submitted these materials to N_2 sorption tests at 77 K (Figure 2f, Table 1). As expected, Zr-**fcu**-azo/sti-10% performed very similarly to the pre-ozonated material, showing only slightly higher values for apparent A_{BET} (3115 m^2/g vs. 3060 m^2/g) and total pore volume (1.32 cm^3/g vs. 1.28 cm^3/g). Based on the Dubinin-Radushkevich (DR) equation,[27] the relative proportion of micro-porosity to the total pore volume was estimated to be 96 % (Figure 2g). Although the washed ozonated Zr-**fcu**-azo/sti-20% showed a nearly identical value for this parameter (95 %), its isotherm exhibited a shoulder/step characteristic from bigger pores, giving insights into the modified nature of the microporosity. The isotherms for the washed ozonated Zr-**fcu**-azo/sti-30% and Zr-**fcu**-azo/sti-40% did not show the type I shape of the isotherms of the corresponding starting MOFs, but rather they exhibited a small hysteresis on the desorption branch, characteristic of mesoporosity (Figures S29, S30). Notably, ozonolysis treatment reduced the apparent A_{BET}: for the washed ozonated Zr-**fcu**-azo/sti-30%, 2680 m^2/g (vs. 3000 m^2/g); and for the washed ozonated Zr-**fcu**-azo/sti-40%, 2580 m^2/g (vs. 3040 m^2/g) (Table 1). However, in both cases, this decrease was offset by a major increase in the proportion of pores with mesoscale dimensions, as derived from the DR equation (Figure 2g and Table S9): for the washed ozonated Zr-**fcu**-azo/sti-30%, 15 % (vs. 2 %); and for the washed ozonated Zr-**fcu**-azo/sti-40%, 24 % (vs. 3 %). Likewise, the total pore volume also increased in both cases: for the washed ozonated Zr-**fcu**-azo/sti-30%, 1.36 cm^3/g (vs. 1.24 cm^3/g) and for the washed ozonated Zr-**fcu**-azo/sti-40%, 1.44 cm^3/g (vs. 1.27 cm^3/g). Similar results were observed in the washed ozonated Zr-**fcu**-azo/sti-50%, which exhibited the most extreme change relative to the corresponding starting MOF: the contribution of the mesoporosity reached 42 % of the total porosity (Figure 2g and Table S9), and the hysteresis characteristic from mesoporosity was clearly visible (Figure S31); consequently, its A_{BET} was only 1860 m^2/g (vs. 3065 m^2/g). Note that additional washing treatment did not affect the sorption properties (Figure S40a), excluding the hypothesis of structural etching sometimes observed through chemical treatment.[18e, 28]

The modification of the micro- vs meso- porosity ratio was also reflected by studying the PSD (Figure 2i). If no noticeable change was observed for the washed ozonated Zr-**fcu**-azo, a subtle appearance of pores of ca. 25 Å and above was noted for the washed ozonated Zr-**fcu**-azo/sti-10%. The washed ozonated Zr-**fcu**-azo/sti-20% and 30% showed a clear decrease of the initial main pore size of ca. 18.4 Å and an increase of the second population at ca. 22.4 Å, confirming that micropores are merged into wider pores. For these two samples, the formation of pores bigger than 25 Å was also visible. Finally, the initial main pores of ca. 18.4 Å completely vanished in washed and ozonated Zr-**fcu**-azo/sti-40% and 50%. In these cases, the pores were mainly observed at ca. 22.4 Å and spread over a wide range up to 50 Å. Albeit non observed through PXRD, the pore population centered at 22.4 Å could be attributed to the existence of non-ordered **reo** motifs, resulting from the removal of inorganic clusters, as hypothesized in some comparable systems.[18e]
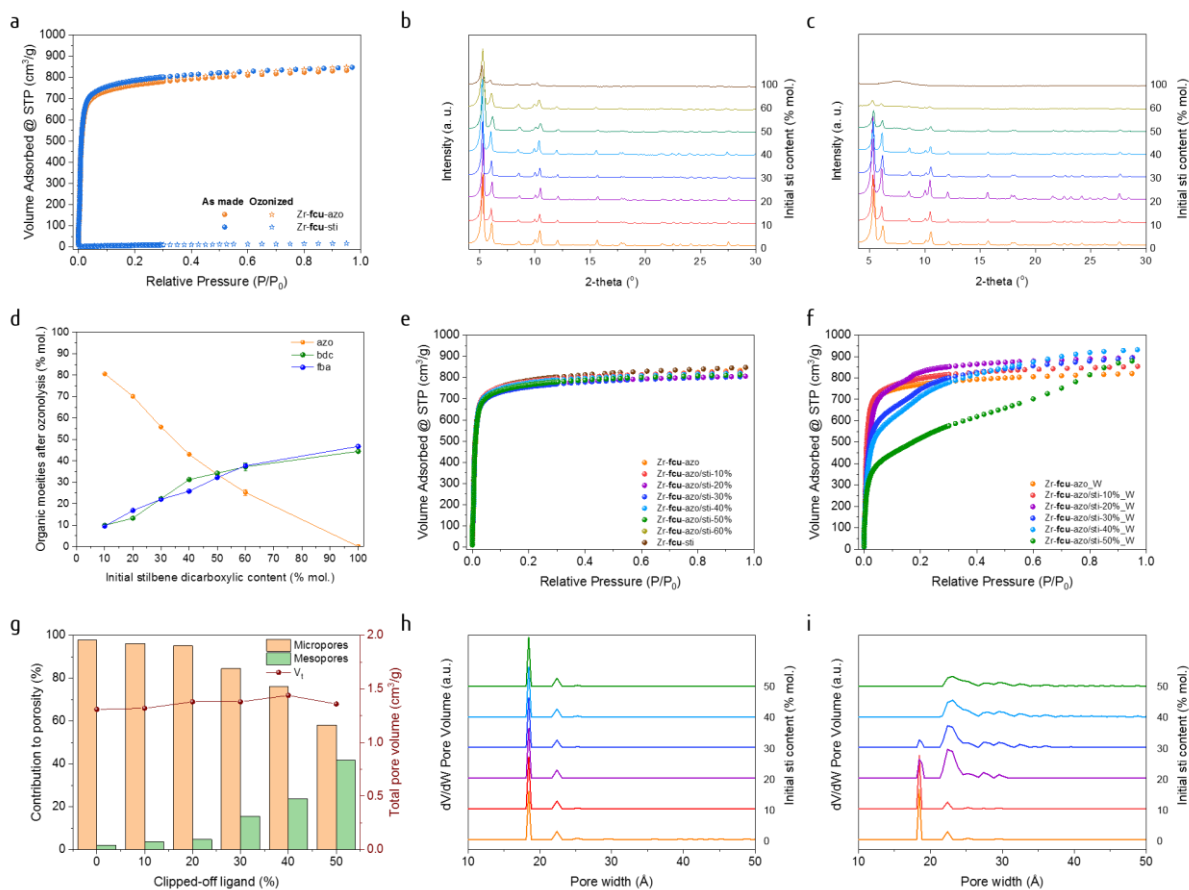
Figure 2. a) N$_2$ sorption isotherms for Zr-**fcu**-azo and Zr-**fcu**-sti before and after ozonolysis. b) PXRD diagrams for Zr-**fcu**-azo/sti-X%. c) PXRD diagrams for ozonated, washed Zr-**fcu**-azo/sti-X%. d) Remaining organic moieties in Zr-**fcu**-azo/sti-X%_OZ, as derived from ^{1}H NMR spectra of digested samples. e) N$_2$ sorption isotherms (77 K) for Zr-**fcu**-azo/sti-X%. f) N$_2$ sorption isotherms (77 K) for ozonated Zr-**fcu**-azo/sti-X% after washing (denoted here by "_W"). g) Change in total pore volume, and in the relative contribution of microporosity and mesoporosity to total uptake, in Zr-**fcu**-azo/sti-X%_OZ after washing, as calculated with the Dubinin-Radushkevich equation. h) Pore size distribution estimated by DFT for Zr-**fcu**-azo/sti-X%. i) Pore size distribution estimated by DFT for ozonated, washed Zr-**fcu**-azo/sti-X%.

Zr-fcu-**bpdc/pdac system.**

Based on these pioneering results, we envisioned extending our method to a more challenging system. We considered that 4,4'-biphenyldicarboxylic acid (H$_2$bpdc) and 1,4-phenylenediacrylic acid (H$_2$pdac), found in the two Zr-**fcu**-MOFs UiO-67 and NU-801, would be a suitable ligand pair, given their geometric (length ≈ 11.3 Å) and chemical properties (*vide supra*). A particularity of H$_2$pdac is its two olefin bonds (Figure 3b), which we reasoned would enable cutting of the ligand into three distinct parts, rather than two, as in H$_2$sti (Scheme S2, Figure S23). In addition, we hypothesized that removal of the central part of the ligand could generate terephthalaldehyde, which could be sublimated under vacuum at moderate temperature -for example, during ozonolysis and/or during a classical pre-sorption activation procedure (Figure 3). That turned out to be correct and, by obviating the washing step, represented a major improvement to our method.
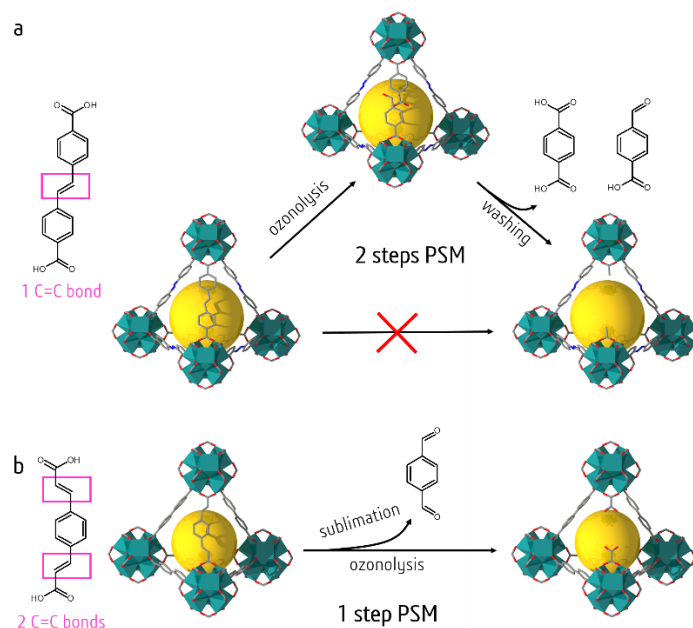
Figure 3. Post-synthetic generation of mesoporosity in MOFs. a) In Zr-**fcu**-azo/sti MOFs, removal of the sti ligand requires two steps: ozonolysis (to break the ligand) and washing. b) In contrast, in Zr-**fcu**-bpdc/pdac MOFs, removal of the pdac ligand requires only one step: ozonolysis (to break the ligand) and concomitant sublimation (to remove the central core). This is made possible by the two olefin groups in this ligand.

Synthesis of Zr-fcu**-bpdc/pdac-X%.** Multivariate Zr-**fcu**-MOFs containing specific ratios of bpdc/pdac, from 100:0 (UiO-67)[14, 29] to 0:100 (NU-801)[19b, 30] were prepared from mixtures of $ZrCl_4$, H_2bpdc and H_2pdac dissolved in DMF in the presence of trifluoroacetic acid, and heated at 120 °C for 72 h in a scintillation vial. The samples were washed with DMF overnight and then soaked in toluene for 3 days. The phase purity of the single crystals of Zr-**fcu**-bpdc/pdac-X% (X ≈ 10, 20, 30, 40% pdac molar percentage) was confirmed by PXRD (Figure 4b), ^{1}H NMR of digested crystals (Figure S24, Table S7) and N_2 sorption analysis performed at 77 K (Figure 4e and Table 2). The sorption isotherms for Zr-**fcu**-bpdc/pdac-X% were comparable (2210 m[2]/g < A_{BET} < 2310 m[2]/g and 0.92 cm[3]/g < Vt < 0.96 cm[3]/g). We observed a slight shoulder at a P/P_0 value of *ca.* 0.1, which we attributed to a higher number of initial defects in the structure, likely due to our use of a slightly different synthetic procedure than for Zr-**fcu**-azo/sti-X%. This is in fact reflected by the estimation of the PSD (Figure 4h), in which all samples presented two main contributions at ca. 15.2 Å and 18.4 Å; the bigger size being attributed (similarly as for Zr-fcu-azo/sti system, *vide supra*) to modulator-related defects.

Table 2. Apparent BET area, microporous and total pore volume of Zr-**fcu**-bpdc/pdac-X%, before and after ozonolysis.

% pdac initial	Starting MOF			Ozonated MOF		
	A_{BET} (m[2]/g)	V_μ (cm[3]/g)	V_t (cm[3]/g)	A_{BET} (m[2]/g)	V_μ (cm[3]/g)	V_t (cm[3]/g)
0	2250	0.91	0.93	2305	0.92	0.95
10	2295	0.95	0.96	2400	0.97	1.09
20	2210	0.91	0.95	1870	0.73	0.99
30	2245	0.93	0.94	1730	0.65	1.05

40	2265	0.93	0.95	Non-porous
100	2310	0.92	0.92	Non-porous

Ozonolysis of Zr-fcu-**bpdc/pdac-X%.** Analogously to the previous MOF pair (*vide supra*), the crystallinity and porosity of UiO-67 were unaffected by ozonolysis (Figures 4a, S11), but cleavage of the pdac ligands in NU-801 led to collapse of its framework and loss of its crystallinity and porosity (Figures 4a, S16). Having demonstrated this, we proceeded with ozonolysis of the Zr-**fcu**-bpdc/pdac-X% MOFs. ^{1}H-NMR of all Zr-**fcu**-bpdc/pdac-X%_OZ highlighted the absence of any remaining pdac ligand (Figures S25, Table S8). Moreover, after the Zr-**fcu**-bpdc/pdac-X%_OZ were activated at 85 °C, a white solid was recovered in the cold trap (77 K) placed between the MOFs and the pump. This solid was confirmed by ^{1}H NMR to be terephthalaldehyde (Figure 4d), which, after cleavage of pdac, we were able to directly extract from the framework via sublimation, as anticipated.

Porosity of Zr-fcu-**bpdc/pdac-X%_OZ.** To investigate the effects of removing the central core of pdac on the porosity of the Zr-**fcu**-bpdc/pdac-X%_OZ, we performed N_2 sorption experiments on these MOFs (Figure 4f, Table 2). Upon extracting terephthalaldehyde from the backbone of Zr-**fcu**-bpdc/pdac-10%, the porosity was enhanced, as demonstrated by an increase in the apparent A_{BET} (from 2295 m^2/g to 2400 m^2/g). In this sample, besides the evolution of microporous pore volume (V_μ) (from 0.95 cm^3/g to 0.97 cm^3/g) was not significant, a more pronounced shoulder in the isotherm reflected a transformation of the microporosity. The emergence of some mesoporosity was revealed by the DR equation, with a contribution of 11 % (vs. 1%) to the total porosity. In contrast, upon further removal of pdac pillars, from Zr-**fcu**-bpdc/pdac-20%_OZ and Zr-**fcu**-bpdc/pdac-30%_OZ, the apparent A_{BET} decreased sharply: for Zr-**fcu**-bpdc/pdac-20%_OZ (A_{BET} = 1870 m^2/g vs. 2210 m^2/g) and for Zr-**fcu**-bpdc/pdac-30%_OZ (A_{BET} = 1730 m^2/g vs. 2245 m^2/g). The loss in microporosity for Zr-**fcu**-bpdc/pdac-20%_OZ ($V\mu$ = 0.73 cm^3/g vs. 0.91 cm^3/g) and for Zr-**fcu**-bpdc/pdac-30%_OZ (V_μ = 0.65 cm^3/g vs. 0.93 cm^3/g) was offset by a major increase in the proportion of pores with mesoscale dimensions, as derived from the DR equation (Figure 4g, Table S10): for Zr-**fcu**-bpdc/pdac-20%_OZ, 26 % (vs. 4%) and for Zr-**fcu**-bpdc/pdac-30%_OZ, 38 % (vs. 1 %). Likewise, the total pore volume also slightly increased in both cases: for Zr-**fcu**-bpdc/pdac-20%_OZ, 0.99 cm^3/g (vs. 0.95 cm^3/g) and for Zr-**fcu**-bpdc/pdac-30%_OZ, 1.05 cm^3/g (vs. 0.94 cm^3/g). As expected, Zr-**fcu**-bpdc/pdac-40%, which, upon ozonation, lost its crystallinity (Figure S15) due to structural collapse caused by removal of 40% of its ligands, was non-porous. Overall, the change in the porosity in Zr-**fcu**-bpdc/pdac-X% paralleled that of Zr-**fcu**-azo/sti-X%. However, in the former, these changes occurred at lower percentages of ligand removal—presumably due to a greater number of defects in the starting MOFs.

The estimation of the PSD in this system also confirmed the evolution of the porosity towards mesopores (Figure 4i). While ozonolysis of UiO-67 did not affect the pore system of the pristine MOF, the appearance of pores distributed between 21.6 Å and 27.4 Å was clearly visible for the ozonated Zr-**fcu**-bpdc/pdac-10%, -20% and -30%. In addition, the two initial main pore populations decreased in ozonated Zr-**fcu**-bpdc/pdac-20% and Zr-**fcu**-bpdc/pdac-30%. In these two last samples, the porosity population was extended up to ca. 50 Å, further confirming the fusion of micropores into novel mesopores.
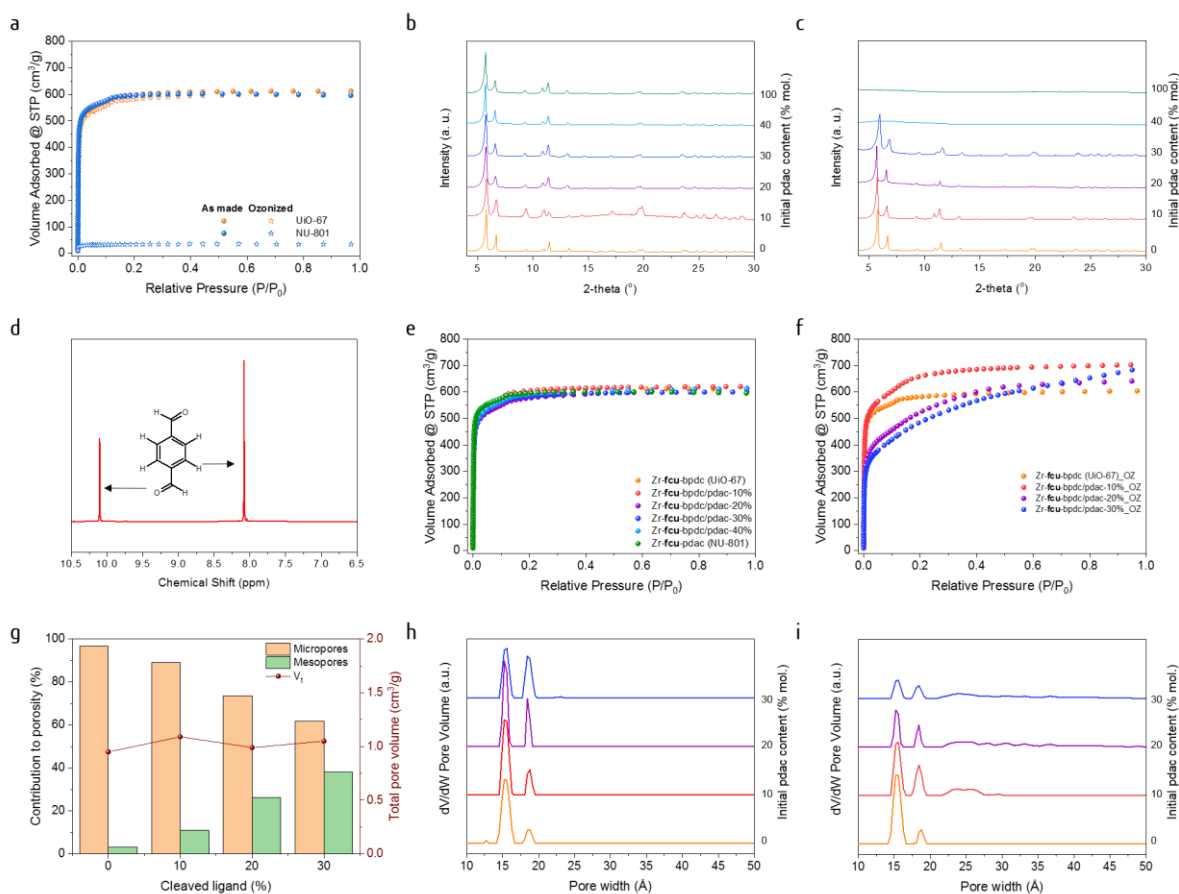
Figure 4. a) N$_2$ sorption isotherms for UiO-67 and NU-801 before and after ozonolysis. b) PXRD diagrams for Zr-**fcu**-bpdc/pdac-X%. c) PXRD diagrams for Zr-**fcu**-bpdc/pdac-X%_OZ. d) ^{1}H NMR spectra of the sublimated terephthalaldehyde recovered by heating at 85 °C under vacuum after ozonolysis. e) N$_2$ sorption isotherms (77 K) for Zr-**fcu**-bpdc/pdac-X%. f) N$_2$ sorption isotherms (77 K) for Zr-**fcu**-bpdc/pdac-X%_OZ. g) Plot showing the overall stability of the total pore volume and evolution of the relative contribution of mesoporosity vs. microporosity to total uptake, in Zr-**fcu**-bpdc/pdac-X%_OZ, as calculated with the Dubinin-Radushkevich equation. h) Pore size distribution estimated by DFT for Zr-**fcu**-bpdc/pdac-X%. i) Pore size distribution estimated by DFT for Zr-**fcu**-bpdc/pdac-X_OZ%.

CONCLUSIONS

In conclusion, we have developed a selective and quantitative method for post-synthetic modification of MOF porosity via ozonolysis. Through removal of organic ligands, our approach causes micropores to fuse into larger (mesoscale) pores in a controlled fashion and without any loss in total porosity. It selectively breaks the olefin bonds in organic ligands without affecting other organic moieties and can be applied for short reaction times (*ca.* 30 min) under mild conditions (room temperature). Moreover, we have demonstrated that ozonolysis can be used as a novel tool to selectively remove, and recover, specific fragments of molecules/frameworks through solid-gas manipulation.

EXPERIMENTAL SECTION

Materials and Instruments

Reagents. 4,4'-stilbenedicarboxylic acid (H$_2$sti), 4,4'-biphenyl dicarboxylic (H$_2$bpdc), and azobenzene-4,4'-dicarboxylic acid (H$_2$azo) were purchased from TCI Europe. Acetic acid, 1,4-phenylenediacrylic (H$_2$pdac), trifluoroacetic acid (tfa), zirconium chloride (ZrCl$_4$), L-proline, hydrochloric acid, potassium iodide and anhydrous granular CaCl$_2$ (2-6 mm) were purchased from Sigma-Aldrich (Merck). *N,N*-dimethylformamide (DMF) and acetone were obtained from Fisher Chemical. Toluene was purchased from Acros Organics. All the reagents and solvents were used as

received. Pyrex tubes (ext Ø =7 mm; in Ø = 5.5 mm; length = 150 mm) were purchased from Vidrasa S.A. The tubes were bent into an L-shape with a flame torch.

Optical Microscopy images were captured by a Zeiss Axio Observer Z1m Optical Microscope.

PXRD diagrams were recorded on an X'Pert PRO MPD analytical diffractometer (Panalytical) at 45 kV, 40 mA using CuKα radiation (λ = 1.5406 Å).

^{1}H NMR spectra were recorded on a Bruker Avance 400 NMR spectrometer (static magnetic field: 11.7 T) operating at Larmor frequencies of 400 MHz (^{1}H).

Ozonolysis treatment was performed using an ozone generator (N1668A from Ozonotec) generating a constant flow of 10.4 mmol/h at room temperature.

Volumetric N_2 sorption isotherms were collected at 77 K (N_2) using an ASAP 2020 HD (Micromeritics). Temperature was controlled by using a liquid nitrogen bath. Total pore volume (V_t) was calculated at P/P_0 = 0.95, and microporous volume (V_μ) was calculated using the Dubinin-Radushkevich equation. Pore size distribution was estimated using a density functional theory (DFT) model (N_2 – cylindrical pores – oxide surface) implemented in the Microactive 4.00 software with a regularization factor of 0.01.

Synthesis.

Synthesis of Zr-fcu**-azo/sti-X%.** 4,4'-stilbenedicarboxylic acid (H_2sti, 0.44-x mmol) and azobenzene-4,4'-dicarboxylic acid (H_2azo, x mmol) were suspended in 10 mL of DMF and sonicated for 30 min in a 23-mL scintillation vial. Then 5 mL of a DMF solution of $ZrCl_4$ (105 mg, 0.45 mmol), L-proline (250 mg, 2.17 mmol) and 45 µL conc. HCl were transferred into the vial and vortexed for 1 minute. After heating at 120 °C for 16 h, the reaction afforded orange octahedral crystals of Zr-**fcu**-azo/sti-X% (see Supporting Information for more details about the H_2azo:H_2sti ratio in this synthesis).

Synthesis of Zr-fcu**-bpdc/pdac-X%.** $ZrCl_4$ (200 mg, 0.86 mmol), 1,4-phenylenediacrylic acid (H_2pdac, x mmol) and biphenyl-4,4'-dicarboxylic acid (H_2bpdc, y mmol) were dissolved by sonication in 10 mL of DMF in the presence of trifluoroacetic acid (tfa, 1 mL) in a 23-mL scintillation vial. After heating at 120 °C for 72 h, colorless octahedral crystals of Zr-**fcu**-bpdc/pdac-X% were obtained (see Supporting Information for more details about the H_2bpdc/H_2pdac ratio in the synthesis).

Sample activation.

Activation of Zr-fcu**-azo/sti-X%.** Crystals of Zr-**fcu**-azo/sti-X% were soaked in 15 mL of DMF (refreshed after 4 h) and then subjected to solvent exchange in 15 mL of acetone (refreshed after 4 h). The supernatant was removed after decantation, and the crystals were dried at 65 °C. Sample purity was verified by PXRD (Figure 2b), and experimental azo/sti ratios were analyzed by ^{1}H NMR of the digested samples (Figure S19, Table S3). Crystals of Zr-**fcu**-azo/sti-X% were then transferred into a glass sorption cell and activated under dynamic vacuum at 85 °C prior to sorption experiments.

Activation of Zr-fcu**-bpdc/pdac-X%.** Crystals of Zr-**fcu**-bpdc/pdac-X% were soaked in 10 mL of DMF for 24 and then subjected to solvent exchange for 72 h in 20 mL of toluene (refreshed twice per day). The supernatant was removed by filtration. The sample purity was verified by PXRD (Figure 4b), and the experimental bpdc/pdac ratios were analyzed by ^{1}H NMR of the digested samples (Figure S24, Table S7). Crystals of Zr-**fcu**-bpdc/pdac-X% were then transferred into a glass sorption cell and activated under dynamic vacuum at 85 °C prior to sorption experiments.

Ozonolysis treatment.

Ozonolysis of the organic ligands. In a typical procedure, 30 mg of the H_2azo, H_2sti, H_2bpdc or H_2pdac were dissolved/dispersed in 20 mL of DMF. The solution was then transferred to a 50 mL

three-necked round bottom flask and was cooled to 0 ℃ using an ice-water bath. A constant ozone flux was blown into the solution through a glass pipette for 30 minutes under stirring. The crude reaction was then allowed to warm up to room temperature and the solvent was removed *in vacuo*. The crude residue was collected and analyzed by ^{1}H NMR. ^{1}H NMR analysis confirmed the inert character of H$_2$azo and H$_2$bpdc, while revealing complete conversion, within 30 minutes, of the active linkers H$_2$sti and H$_2$pdac.

Ozonolysis of Zr-fcu**-azo/sti-X% and Zr-fcu-bpdc/pdac_X%.** A column of Zr-**fcu**-azo/sti-X% or Zr-**fcu**-azo/sti-X% (50 mg to 100 mg) was loaded over a cotton stopper in an L-shaped Pyrex tube. The glass tube was connected to the solid-gas post synthetic modification set-up and purged under vacuum for 5 min. The ozone gas flow (10.4 mmol/h) was passed through the MOF column for 30 min. After 1-2 min, the aqueous potassium iodide solution turned yellow, indicating the whole MOF column had been exposed to ozone atmosphere. The recovered Zr-**fcu**-azo/sti-X%_OZ or Zr-**fcu**-bpdc/pdac-X%_OZ samples were further characterized by PXRD (Figures S10b, S17b) and ^{1}H NMR (Figures S20, S25, Table S4, S8).

Acetic acid wash.

About 50 mg of Zr-**fcu**-azo/sti-X%_OZ were vortexed for a few seconds in 20 mL of a 0.5 M acetic acid solution in DMF and left at room temperature for 24 h. The supernatant was removed and analyzed by ^{1}H NMR after decantation (Figure S22, Table S6). The crystals were washed twice with 20 mL of acetone. The acetone was removed after decantation, and the crystals were dried at 65 ℃. The sample purity was verified by PXRD (Figure S10c), and the experimental organic content was analyzed by ^{1}H NMR of the digested samples (Figures S21, Table S5). Crystals of washed ozonated Zr-**fcu**-azo/sti-X% were then transferred into a glass sorption cell and activated under dynamic vacuum at 85 ℃ prior to the sorption experiments. Note that the Zr-**fcu**-bpdc/pdac-X% samples did not require this additional treatment to reveal their tuned porosity potential (Figures 3, S40b).

HF-Digestion methodology.

In a typical procedure, 10 mg of MOF were placed in an Eppendorf tube, to which 120 μL of a 5% aq. HF solution were added. The mixture was sonicated for 15 minutes, and then the slurry was placed in a 110 ℃ sand bath inside a fume hood to evaporate overnight. The crude solid samples were highly soluble in DMSO-d^6 without any need for addition of acid. Note that attempts with standard digestion methodologies were not successful, even when using the same quantities of HF and solvent. Therefore, the evaporation step is crucial for proper sample digestion. Moreover, the digested solutions obtained with our methodology did not require any specific (*e.g.* HF-resistant) PTFE NMR tubes.

ASSOCIATED CONTENT

Supporting Information. Detailed synthetic procedures, microscopy, PXRD, ^{1}H NMR, additional sorption data. This material is available free of charge via the Internet at http://pubs.acs.org.

AUTHOR INFORMATION

Corresponding Author

* inhar.imaz@icn2.cat

* daniel.maspoch@icn2.cat

Author Contributions

The manuscript was written through contributions of all authors.

ACKNOWLEDGMENT

ABBREVIATIONS

^{1}H NMR, proton nuclear magnetic resonance; A_{BET}, Brunauer-Emmett-Teller area; bdc, terephthalic acid; DFT, density functional theory; DMF, *N,N'*-dimethylformamide; DR, Dubinin-Radushkevich; fba, formylbenzoic acid; H$_2$azo4,4'-azobenzene dicarboxylic acid; H$_2$bpdc, 4,4'-biphenyldicarboxylic acid; H$_2$pdac, 1,4-phenylenediacrylic acid; H$_2$sti, 4,4'-stilbene dicarboxylic acid (H$_2$sti);. HKUST, Hong-Kong university of science and technology; IRMOF, isoreticular metal-organic framework; MIL, material institute Lavoisier; MOF, metal-organic framework; MTV, multivariate; OZ, ozonated; PSD, pore size distribution; PSM, post synthetic modification; PXRD, powder X-ray diffraction; tfa, trifluoroacetic acid; UiO, Universitetet i Oslo; W, washed.

REFERENCES

1. (a) Subramanian, S.; Zaworotko, M. J., Porous Solids by Design: [Zn(4,4'-bpy)$_2$(SiF$_6$)]$_n$·xDMF, a Single Framework Octahedral Coordination Polymer with Large Square Channels, *Angew. Chem., Int. Ed.* **1995,** *34* (19), 2127-2129; (b) Kondo, M.; Yoshitomi, T.; Matsuzaka, H.; Kitagawa, S.; Seki, K., Three-Dimensional Framework with Channeling Cavities for Small Molecules: {[M2(4, 4'-bpy)3(NO3)4]·xH2O}n (M □ Co, Ni, Zn), *Angew. Chem. Int. Ed.* **1997,** *36* (16), 1725-1727; (c) Li, H.; Eddaoudi, M.; O'Keeffe, M.; Yaghi, O. M., Design and synthesis of an exceptionally stable and highly porous metal-organic framework, *Nature* **1999,** *402* (6759), 276-279; (d) Eddaoudi, M.; Kim, J.; Rosi, N.; Vodak, D.; Wachter, J.; O'Keeffe, M.; Yaghi, O. M., Systematic Design of Pore Size and Functionality in Isoreticular MOFs and Their Application in Methane Storage, *Science* **2002,** *295* (5554), 469-472; (e) Chui, S. S. Y.; Lo, S. M. F.; Charmant, J. P. H.; Orpen, A. G.; Williams, I. D., A chemically functionalizable nanoporous material [Cu3(TMA)2(H2O)3]n, *Science* **1999,** *283* (5405), 1148-1150.

2. (a) Zhou, H. C.; Kitagawa (Eds.), S., Themed issue: Metal-Organic Frameworks, *Chem. Soc. Rev.,* **2014***, 43, *(5), 5415-6172; (b) Zhou, H. C.; Long, J. R.; Yaghi (Eds.), O. M., Themed issue: Metal-Organic Frameworks, *Chem. Rev.,* **2012***, 112, *(2), 673-1268; (c) Long, J. R.; Yaghi (Eds.), O. M., Themed issue: Metal-Organic Frameworks, *Chem. Soc. Rev.,* **2009***, 38, *(5), 1201-1508

3. (a) Suh, M. P.; Park, H. J.; Prasad, T. K.; Lim, D.-W., Hydrogen Storage in Metal–Organic Frameworks, *Chem. Rev.* **2012,** *112* (2), 782-835; (b) He, Y.; Zhou, W.; Qian, G.; Chen, B., Methane storage in metal-organic frameworks, *Chem. Soc. Rev.* **2014,** *43* (16), 5657-5678; (c) Sumida, K.; Rogow, D. L.; Mason, J. A.; McDonald, T. M.; Bloch, E. D.; Herm, Z. R.; Bae, T.-H.; Long, J. R., Carbon Dioxide Capture in Metal–Organic Frameworks, *Chem. Rev.* **2012,** *112* (2), 724-781.

4. Farrusseng, D.; Aguado, S.; Pinel, C., Metal–Organic Frameworks: Opportunities for Catalysis, *Angew. Chem., Int. Ed.* **2009,** *48* (41), 7502-7513.

5. Horcajada, P.; Gref, R.; Baati, T.; Allan, P. K.; Maurin, G.; Couvreur, P.; Férey, G.; Morris, R. E.; Serre, C., Metal–Organic Frameworks in Biomedicine, *Chem. Rev.* **2012,** *112* (2), 1232-1268.

6.   de Lange, M. F.; Verouden, K. J. F. M.; Vlugt, T. J. H.; Gascon, J.; Kapteijn, F., Adsorption-Driven Heat Pumps: The Potential of Metal–Organic Frameworks, *Chem. Rev.* **2015,** *115* (22), 12205-12250.

7.   Kreno, L. E.; Leong, K.; Farha, O. K.; Allendorf, M.; Van Duyne, R. P.; Hupp, J. T., Metal–Organic Framework Materials as Chemical Sensors, *Chem. Rev.* **2012,** *112* (2), 1105-1125.

8.   Belmabkhout, Y.; Guillerm, V.; Eddaoudi, M., Low concentration CO_2 capture using physical adsorbents: Are metal–organic frameworks becoming the new benchmark materials?, *Chem. Eng. J.* **2016,** *296*, 386-397.

9.   (a) Cohen, S. M., Postsynthetic Methods for the Functionalization of Metal-Organic Frameworks, *Chem. Rev.* **2012,** *112* (2), 970-1000; (b) Kim, M.; Cohen, S. M., Discovery, development, and functionalization of Zr(iv)-based metal–organic frameworks, *CrystEngComm* **2012,** *14* (12), 4096-4104; (c) Bloch, W. M.; Burgun, A.; Coghlan, C. J.; Lee, R.; Coote, M. L.; Doonan, C. J.; Sumby, C. J., Capturing snapshots of post-synthetic metallation chemistry in metal–organic frameworks, *Nat. Chem.* **2014,** *6*, 906; (d) Garibay, S. J.; Cohen, S. M., Isoreticular synthesis and modification of frameworks with the UiO-66 topology, *Chem. Commun.* **2010,** *46* (41), 7700-7702.

10.   (a) Yaghi, O. M.; O'Keeffe, M.; Ockwig, N. W.; Chae, H. K.; Eddaoudi, M.; Kim, J., Reticular synthesis and the design of new materials, *Nature* **2003,** *423* (6941), 705-714; (b) Chae, H. K.; Eddaoudi, M.; Kim, J.; Hauck, S. I.; Hartwig, J. F.; O'Keeffe, M.; Yaghi, O. M., Tertiary Building Units: Synthesis, Structure, and Porosity of a Metal−Organic Dendrimer Framework (MODF-1)⊥, *J. Am. Chem. Soc.* **2001,** *123* (46), 11482-11483; (c) Eddaoudi, M.; Moler, D. B.; Li, H. L.; Chen, B. L.; Reineke, T. M.; O'Keeffe, M.; Yaghi, O. M., Modular chemistry: Secondary building units as a basis for the design of highly porous and robust metal-organic carboxylate frameworks, *Acc. Chem. Res.* **2001,** *34* (4), 319-330; (d) Eddaoudi, M.; Kim, J.; O'Keeffe, M.; Yaghi, O. M., $Cu_2[o$-Br-$C_6H_3(CO_2)_2]_2(H_2O)_2·(DMF)_8(H_2O)_2$: A Framework Deliberately Designed To Have the NbO Structure Type, *J. Am. Chem. Soc.* **2002,** *124* (3), 376-377; (e) Deng, H.; Grunder, S.; Cordova, K. E.; Valente, C.; Furukawa, H.; Hmadeh, M.; Gándara, F.; Whalley, A. C.; Liu, Z.; Asahina, S.; Kazumori, H.; O'Keeffe, M.; Terasaki, O.; Stoddart, J. F.; Yaghi, O. M., Large-Pore Apertures in a Series of Metal-Organic Frameworks, *Science* **2012,** *336* (6084), 1018-1023; (f) Furukawa, H.; Cordova, K. E.; O'Keeffe, M.; Yaghi, O. M., The Chemistry and Applications of Metal-Organic Frameworks, *Science* **2013,** *341* (6149); (g) Guillerm, V.; Grancha, T.; Imaz, I.; Juanhuix, J.; Maspoch, D., Zigzag Ligands for Transversal Design in Reticular Chemistry: Unveiling New Structural Opportunities for Metal–Organic Frameworks, *J. Am. Chem. Soc.* **2018,** *140* (32), 10153-10157.

11.   (a) Li, P.; Vermeulen, N. A.; Malliakas, C. D.; Gómez-Gualdrón, D. A.; Howarth, A. J.; Mehdi, B. L.; Dohnalkova, A.; Browning, N. D.; O'Keeffe, M.; Farha, O. K., Bottom-up construction of a superstructure in a porous uranium-organic crystal, *Science* **2017,** *356* (6338), 624-627; (b) Farha, O. K.; Eryazici, I.; Jeong, N. C.; Hauser, B. G.; Wilmer, C. E.; Sarjeant, A. A.; Snurr, R. Q.; Nguyen, S. T.; Yazaydin, A. Ö.; Hupp, J. T., Metal-Organic Framework Materials with Ultrahigh Surface Areas: Is the Sky the Limit?, *J. Am. Chem. Soc.* **2012,** *134* (36), 15016-15021; (c) Férey, G.; Mellot-Draznieks, C.; Serre, C.; Millange, F.; Dutour, J.; Surblé, S.; Margiolaki, I., A chromium terephthalate-based solid with unusually large pore volumes and surface area, *Science* **2005,** *309* (5743), 2040-2042; (d) Guillerm, V.; Weseliński, Ł. J.; Belmabkhout, Y.; Cairns, A. J.; D'Elia, V.; Wojtas, Ł.; Adil, K.; Eddaoudi, M., Discovery and introduction of a (3,18)-connected net as an ideal blueprint for the design of metal-organic frameworks, *Nat. Chem.* **2014,** *6* (8), 673-680.

12.   (a) Seki, K.; Takamizawa, S.; Mori, W., Design and Gas Adsorption Property of a Three-Dimensional Coordination Polymer with a Stable and Highly Porous Framework, *Chem. Letters* **2001,** *30* (4), 332-333; (b) Nugent, P.; Belmabkhout, Y.; Burd, S. D.; Cairns, A. J.; Luebke, R.; Forrest, K.;

Pham, T.; Ma, S.; Space, B.; Wojtas, Ł.; Eddaoudi, M.; Zaworotko, M. J., Porous materials with optimal adsorption thermodynamics and kinetics for CO_2 separation, *Nature* **2013,** *495* (7439), 80-84.

13.   Sun, D.; Ma, S.; Ke, Y.; Collins, D. J.; Zhou, H.-C., An Interweaving MOF with High Hydrogen Uptake, *J. Am. Chem. Soc.* **2006,** *128* (12), 3896-3897.

14.   (a) Cavka, J. H.; Jakobsen, S.; Olsbye, U.; Guillou, N.; Lamberti, C.; Bordiga, S.; Lillerud, K. P., A new zirconium inorganic building brick forming metal organic frameworks with exceptional stability, *J. Am. Chem. Soc.* **2008,** *130* (42), 13850-13851; (b) Schaate, A.; Roy, P.; Godt, A.; Lippke, J.; Waltz, F.; Wiebcke, M.; Behrens, P., Modulated Synthesis of Zr- Based Metal–Organic Frameworks: From Nano to Single Crystals, *Chem. Eur. J.* **2011,** *17* (24), 6643-6651.

15.   (a) Serre, C.; Mellot-Draznieks, C.; Surblé, S.; Audebrand, N.; Filinchuk, Y.; Férey, G., Role of solvent-host interactions that lead to very large swelling of hybrid frameworks, *Science* **2007,** *315* (5820), 1828-1831; (b) Dan-Hardi, M.; Chevreau, H.; Devic, T.; Horcajada, P.; Maurin, G.; Férey, G.; Popov, D.; Riekel, C.; Wuttke, S.; Lavalley, J.-C.; Vimont, A.; Boudewijns, T.; de Vos, D.; Serre, C., How Interpenetration Ensures Rigidity and Permanent Porosity in a Highly Flexible Hybrid Solid, *Chem. Mater.* **2012,** *24* (13), 2486-2492.

16.   Eubank, J. F.; Nouar, F.; Luebke, R.; Cairns, A. J.; Wojtas, Ł.; Alkordi, M.; Bousquet, T.; Hight, M. R.; Eckert, J.; Embs, J. P.; Georgiev, P. A.; Eddaoudi, M., On Demand: The Singular rht Net, an Ideal Blueprint for the Construction of a Metal–Organic Framework (MOF) Platform, *Angew. Chem., Int. Ed.* **2012,** *51* (40), 10099-10103.

17.   (a) Sonnauer, A.; Hoffmann, F.; Froeba, M.; Kienle, L.; Duppel, V.; Thommes, M.; Serre, C.; Férey, G.; Stock, N., Giant Pores in a Chromium 2,6-Naphthalenedicarboxylate Open-Framework Structure with MIL-101 Topology, *Angew. Chem., Int. Ed.* **2009,** *48* (21), 3791-3794; (b) Koh, K.; Wong-Foy, A. G.; Matzger, A. J., A Crystalline Mesoporous Coordination Copolymer with High Microporosity, *Angew. Chem., Int. Ed.* **2008,** *47* (4), 677-680; (c) Feng, D.; Wang, K.; Su, J.; Liu, T.-F.; Park, J.; Wei, Z.; Bosch, M.; Yakovenko, A.; Zou, X.; Zhou, H.-C., A Highly Stable Zeotype Mesoporous Zirconium Metal–Organic Framework with Ultralarge Pores, *Angew. Chem., Int. Ed.* **2015,** *54* (1), 149-154; (d) Serra-Crespo, P.; Ramos-Fernandez, E. V.; Gascon, J.; Kapteijn, F., Synthesis and Characterization of an Amino Functionalized MIL-101(Al): Separation and Catalytic Properties, *Chem. Mater.* **2011,** *23* (10), 2565-2572; (e) Feng, L.; Yuan, S.; Zhang, L.-L.; Tan, K.; Li, J.-L.; Kirchon, A.; Liu, L.-M.; Zhang, P.; Han, Y.; Chabal, Y. J.; Zhou, H.-C., Creating Hierarchical Pores by Controlled Linker Thermolysis in Multivariate Metal–Organic Frameworks, *J. Am. Chem. Soc.* **2018,** *140* (6), 2363-2372.

18.   (a) Cliffe, M. J.; Wan, W.; Zou, X.; Chater, P. A.; Kleppe, A. K.; Tucker, M. G.; Wilhelm, H.; Funnell, N. P.; Coudert, F.-X.; Goodwin, A. L., Correlated defect nanoregions in a metal–organic framework, *Nat. Commun.* **2014,** *5*, 4176; (b) N., B. D.; R., D. W., Mixed Linker Strategies for Organic Framework Functionalization, *Chem. Eur. J.* **2013,** *19* (3), 818-827; (c) Park, J.; Wang, Z. U.; Sun, L.-B.; Chen, Y.-P.; Zhou, H.-C., Introduction of Functionalized Mesopores to Metal–Organic Frameworks via Metal–Ligand–Fragment Coassembly, *J. Am. Chem. Soc.* **2012,** *134* (49), 20110-20116; (d) Choi, K. M.; Jeon, H. J.; Kang, J. K.; Yaghi, O. M., Heterogeneity within Order in Crystals of a Porous Metal–Organic Framework, *J. Am. Chem. Soc.* **2011,** *133* (31), 11920-11923; (e) Yuan, S.; Zou, L.; Qin, J.-S.; Li, J.; Huang, L.; Feng, L.; Wang, X.; Bosch, M.; Alsalme, A.; Cagin, T.; Zhou, H.-C., Construction of hierarchically porous metal–organic frameworks through linker labilization, *Nat. Commun.* **2017,** *8*, 15356; (f) Fang, Z.; Bueken, B.; De Vos, D. E.; Fischer, R. A., Defect-Engineered Metal–Organic Frameworks, *Angew. Chem., Int. Ed.* **2015,** *54* (25), 7234-7254; (g) Bradshaw, D.; El-Hankari, S.; Lupica-Spagnolo, L., Supramolecular templating of hierarchically porous metal–organic frameworks, *Chem. Soc. Rev.* **2014,** *43* (16), 5431-5443; (h) Liang, W.; Coghlan, C. J.; Ragon, F.; Rubio-Martinez, M.; D'Alessandro, D. M.; Babarao, R., Defect engineering

of UiO-66 for CO_2 and H_2O uptake – a combined experimental and simulation study, *Dalton Trans.* **2016,** *45* (11), 4496-4500.

19.   (a) Wißmann, G.; Schaate, A.; Lilienthal, S.; Bremer, I.; Schneider, A. M.; Behrens, P., Modulated synthesis of Zr-fumarate MOF, *Microporous Mesoporous Mater.* **2012,** *152*, 64-70; (b) Gutov, O. V.; Molina, S.; Escudero- Adán, E. C.; Shafir, A., Modulation by Amino Acids: Toward Superior Control in the Synthesis of Zirconium Metal–Organic Frameworks, *Chem. Eur. J.* **2016,** *22* (38), 13582-13587; (c) Marshall, R. J.; Hobday, C. L.; Murphie, C. F.; Griffin, S. L.; Morrison, C. A.; Moggach, S. A.; Forgan, R. S., Amino acids as highly efficient modulators for single crystals of zirconium and hafnium metal-organic frameworks, *J. Mater. Chem. A* **2016,** *4* (18), 6955-6963; (d) Øien, S.; Wragg, D.; Reinsch, H.; Svelle, S.; Bordiga, S.; Lamberti, C.; Lillerud, K. P., Detailed Structure Analysis of Atomic Positions and Defects in Zirconium Metal–Organic Frameworks, *Cryst. Growth Des.* **2014,** *14* (11), 5370-5372; (e) Trickett, C. A.; Gagnon, K. J.; Le, e. S.; Gándara, F.; Bürgi, H.-B.; Yaghi, O. M., Definitive Molecular Level Characterization of Defects in UiO-66 Crystals, *Angew. Chem., Int. Ed.* **2015,** *54* (38), 11162-11167.

20.   (a) Yue, Y.; Qiao, Z.-A.; Fulvio, P. F.; Binder, A. J.; Tian, C.; Chen, J.; Nelson, K. M.; Zhu, X.; Dai, S., Template-Free Synthesis of Hierarchical Porous Metal–Organic Frameworks, *J. Am. Chem. Soc.* **2013,** *135* (26), 9572-9575; (b) Yue, Y.; Fulvio, P. F.; Dai, S., Hierarchical Metal–Organic Framework Hybrids: Perturbation-Assisted Nanofusion Synthesis, *Acc. Chem. Res.* **2015,** *48* (12), 3044-3052; (c) Sun, L.-B.; Li, J.-R.; Park, J.; Zhou, H.-C., Cooperative Template-Directed Assembly of Mesoporous Metal–Organic Frameworks, *J. Am. Chem. Soc.* **2012,** *134* (1), 126-129; (d) Huang, H.; Li, J.-R.; Wang, K.; Han, T.; Tong, M.; Li, L.; Xie, Y.; Yang, Q.; Liu, D.; Zhong, C., An in situ self-assembly template strategy for the preparation of hierarchical-pore metal-organic frameworks, *Nat. Commun.* **2015,** *6*, 8847; (e) Qiu, L.-G.; Xu, T.; Li, Z.-Q.; Wang, W.; Wu, Y.; Jiang, X.; Tian, X.-Y.; Zhang, L.-D., Hierarchically Micro- and Mesoporous Metal–Organic Frameworks with Tunable Porosity, *Angew. Chem., Int. Ed.* **2008,** *47* (49), 9487-9491; (f) Zhao, Y.; Zhang, J.; Han, B.; Song, J.; Li, J.; Wang, Q., Metal–Organic Framework Nanospheres with Well-Ordered Mesopores Synthesized in an Ionic Liquid/CO_2/Surfactant System, *Angew. Chem., Int. Ed.* **2011,** *50* (3), 636-639; (g) Cao, S.; Gody, G.; Zhao, W.; Perrier, S.; Peng, X.; Ducati, C.; Zhao, D.; Cheetham, A. K., Hierarchical bicontinuous porosity in metal–organic frameworks templated from functional block co-oligomer micelles, *Chem. Sci.* **2013,** *4* (9), 3573-3577; (h) Wee, L. H.; Wiktor, C.; Turner, S.; Vanderlinden, W.; Janssens, N.; Bajpe, S. R.; Houthoofd, K.; Van Tendeloo, G.; De Feyter, S.; Kirschhock, C. E. A.; Martens, J. A., Copper Benzene Tricarboxylate Metal–Organic Framework with Wide Permanent Mesopores Stabilized by Keggin Polyoxometallate Ions, *J. Am. Chem. Soc.* **2012,** *134* (26), 10911-10919; (i) Shen, K.; Zhang, L.; Chen, X.; Liu, L.; Zhang, D.; Han, Y.; Chen, J.; Long, J.; Luque, R.; Li, Y.; Chen, B., Ordered macro-microporous metal-organic framework single crystals, *Science* **2018,** *359* (6372), 206-210.

21.   Albalad, J.; Xu, H.; Gándara, F.; Haouas, M.; Martineau-Corcos, C.; Mas-Ballesté, R.; Barnett, S. A.; Juanhuix, J.; Imaz, I.; Maspoch, D., Single-Crystal-to-Single-Crystal Postsynthetic Modification of a Metal–Organic Framework via Ozonolysis, *J. Am. Chem. Soc.* **2018,** *140* (6), 2028-2031.

22.   (a) Geletneky, C.; Berger, S., The Mechanism of Ozonolysis Revisited by ^{17}O-NMR Spectroscopy, *Eur. J. Org. Chem.* **1998,** *1998* (8), 1625-1627; (b) Criegee, R., Mechanism of Ozonolysis, *Angew. Chem., Int. Ed.* **1975,** *14* (11), 745-752.

23.   Deng, H.; Doonan, C. J.; Furukawa, H.; Ferreira, R. B.; Towne, J.; Knobler, C. B.; Wang, B.; Yaghi, O. M., Multiple Functional Groups of Varying Ratios in Metal-Organic Frameworks, *Science* **2010,** *327* (5967), 846-850.

24.   (a) Marshall, R. J.; Forgan, R. S., Postsynthetic Modification of Zirconium Metal-Organic Frameworks, *Eur. J. Inorg. Chem.* **2016,** (27), 4310-4331; (b) Ragon, F.; Campo, B.; Yang, Q.; Martineau, C.; Wiersum, A. D.; Lago, A.; Guillerm, V.; Hemsley, C.; Eubank, J. F.; Vishnuvarthan, M.; Taulelle, F.; Horcajada, P.; Vimont, A.; Llewellyn, P. L.; Daturi, M.; Devautour-Vinot, S.; Maurin, G.; Serre, C.; Devic, T.; Clet, G., Acid-functionalized UiO-66(Zr) MOFs and their evolution after intra-framework cross-linking: structural features and sorption properties, *J. Mater. Chem. A* **2015,** *3* (7), 3294-3309.

25.   (a) Yang, Q.; Guillerm, V.; Ragon, F.; Wiersum, A. D.; Llewellyn, P. L.; Zhong, C.; Devic, T.; Serre, C.; Maurin, G., CH_4 storage and CO_2 capture in highly porous zirconium oxide based metal-organic frameworks, *Chem. Commun.* **2012,** *48* (79), 9831-9833; (b) Hobday, C. L.; Marshall, R. J.; Murphie, C. F.; Sotelo, J.; Richards, T.; Allan, D. R.; Düren, T.; Coudert, F.-X.; Forgan, R. S.; Morrison, C. A.; Moggach, S. A.; Bennett, T. D., A Computational and Experimental Approach Linking Disorder, High-Pressure Behavior, and Mechanical Properties in UiO Frameworks, *Angew. Chem., Int. Ed.* **2016,** *55* (7), 2401-2405.

26.   Marshall, R. J.; Richards, T.; Hobday, C. L.; Murphie, C. F.; Wilson, C.; Moggach, S. A.; Bennett, T. D.; Forgan, R. S., Postsynthetic bromination of UiO-66 analogues: altering linker flexibility and mechanical compliance, *Dalton Trans.* **2016,** *45* (10), 4132-4135.

27.   Dubinin, M. M.; Zaverina, E. D.; Radushkevich, L. V., Sorbtsiya I Struktura Aktivnykh Uglei .1. Issledovanie Adsorbtsii Organicheskikh Parov, *Zh. Fiz. Khim.* **1947,** *21* (11), 1351-1362.

28.   Avci, C.; Ariñez-Soriano, J.; Carné-Sánchez, A.; Guillerm, V.; Carbonell, C.; Imaz, I.; Maspoch, D., Post-Synthetic Anisotropic Wet-Chemical Etching of Colloidal Sodalite ZIF Crystals, *Angew. Chem., Int. Ed.* **2015,** *54* (48), 14417-14421.

29.   Guillerm, V.; Ragon, F.; Dan-Hardi, M.; Devic, T.; Vishnuvarthan, M.; Campo, B.; Vimont, A.; Clet, G.; Yang, Q.; Maurin, G.; Férey, G.; Vittadini, A.; Gross, S.; Serre, C., A series of isoreticular, highly stable, porous zirconium oxide based metal-organic frameworks, *Angew. Chem., Int. Ed.* **2012,** *51* (37), 9267-71.

30.   Gomez-Gualdron, D. A.; Gutov, O. V.; Krungleviciute, V.; Borah, B.; Mondloch, J. E.; Hupp, J. T.; Yildirim, T.; Farha, O. K.; Snurr, R. Q., Computational Design of Metal–Organic Frameworks Based on Stable Zirconium Building Units for Storage and Delivery of Methane, *Chem. Mater.* **2014,** *26* (19), 5632-5639.